Colloid Polym Sci (2009) 287:13–22
DOI 10.1007/s00396-008-1950-7

ORIGINAL CONTRIBUTION

# Synthesis and aggregation study of tin nanoparticles and colloids obtained by chemical liquid deposition

**M. F. Meléndrez · G. Cárdenas · J. Díaz V · C. Cruzat C · J. Arbiol**

Received: 4 August 2008 / Revised: 7 October 2008 / Accepted: 15 October 2008 / Published online: 12 November 2008


**Abstract** Tin colloids (Sn-Colls) and nanoparticles were synthesized by a chemical liquid deposition method (CLD). $Sn^0$ was evaporated and codeposited with acetone, 2-propanol, and tetrahydrofurane vapors at 77 K to obtain colloidal dispersions. Sn-Coll were characterized by UV spectroscopy, transmission electron microscopy (TEM), high resolution transmission electron microscopy, selected area electron diffraction, thermal analysis, infrared spectroscopy [Fourier transform infrared (FTIR)], and light scattering. TEM micrographs of tin nanoparticles (Sn-Nps) revealed a particle size distribution between 2 and 4 nm for the three solvents used in the synthesis. UV studies showed strong absorption bands in the UV region, suggesting that the Sn-Nps obtained by CLD exhibit quantum confinement and typical bands of plasmons corresponded to aggregated particles. Electrophoresis measurement indicated a significant tendency of particle aggregation along time, which was verified by light scattering studies. The diffraction patterns revealed phases corresponding to metallic tin and FTIR studies showed the interaction Sn-solvent in the metal surface by Sn-O bonds, indicating a solvatation of metallic clusters. Thermal analysis revealed a good thermal stability of Sn-Nps. The mechanism of tin nanoparticles formation was also examined.

M. F. Meléndrez · G. Cárdenas (✉) · J. Díaz V · C. Cruzat C
Department of Polymers, Advanced Materials Laboratory,
Universidad de Concepción,
P.O. Box, 160-C, Concepcion, Chile
e-mail: galocardenas@udec.cl

M. F. Meléndrez
e-mail: mmelendrez@udec.cl

J. Arbiol
TEM-MAT, Serveis Scientificotecnics, Universitat de Barcelona,
08028, Barcelona, Catalonia, Spain

**Keywords** Nanoparticles · Colloids · Vapor deposition · Fractal aggregates

## Introduction

Due to the potential application in diverse fields, metal nanoparticles have attracted great attention in recent years [1]. These ultrafine particles often exhibit unusual physical and chemical properties that are distinct from either simple molecules or bulk materials. Current research in this area is motivated by the possible application of these unique properties. Although many methods, such as chemical reduction [2, 4], metal vapor deposition [5], electrochemical synthesis [6], thermal decomposition [7], and microwave irradiation [8], have been used to prepare metal nanoparticles, all of these techniques cannot be used to produce metal nanoparticles on a large scale [9]. Most synthesis methods present disadvantages in the purification of particles; therefore, chemical liquid deposition (CLD) offers an ideal method for the preparation of metallic nanoparticles by the codeposition of metallic vapors with organic solvents that stabilize the colloidal systems, producing smaller particles free of impurities. This method has been studied by Klabunde [10–12] and Cárdenas [13].

From CLD, Pd, Au, Ni, Zn, Cd, Zn, Mo, Fe, Co, and Ag nanostructured materials have been prepared [14, 15]. The synthesis study of Sn-Nps allows one to understand the particle agglomeration in colloidal systems and the effect of interband transition due to plasmon absorption [16]. This is also an important source to obtain $SnO_2$ thin films by their optical, chemical, and electric properties [17, 18]. Another way to synthesize metallic-Nps is by metallic vapor condensation (MVC) directly over frozen substrate at 77 K. This technique does not produce particle stabilization

because the reaction is carried out without solvents. Maintaining a good control of substrate and evaporation pressure, nanoparticles can be deposited in substrates, forming ultrathin films. Tin colloids (Sn-Coll) and depositions are produced by both methods (CLD and MVC). For subsequent oxidation of Sn-Colls, $SnO_2$ colloidal nanoparticles can be obtained by application of optoelectronic and sensor devices, among others [19]. In terms of control of particle size distribution, fractal aggregate formation and stabilization of particles by solvatation with organic molecules, CLD easily outperforms any of the other techniques, and this is why this technique is a very useful method in the production of metallic-Nps.

The aim of this work was to synthesize Sn-Nps by CLD with stabilizing solvents. Effects of metal–solvent interaction in the stabilization of colloidal systems, particle size, aggregation, and thermal stability of colloids and nanoparticles were studied. The control of these processes would permit the application of Sn-Nps in printing electronic circuits.

## Experimental

### Synthesis of Sn-coll by CLD

Tin colloids were prepared by CLD method [20], which involves the vapor deposition of metallic Sn in organic vapor media. The metallic atom reactions were carried out in a glass reactor. A W-$Al_2O_3$ crucible loaded with Sn was assembled in the metallic atom reactor and the whole system was evacuated. A glass device with organic solvents (2-propanol, acetone, and THF p.a. grade, purchased from Fisher, Pittsburgh, PA, USA), dried with molecular sieves and further degasified three times by standard freeze–thaw procedure [20], was attached to the neck of the reactor. The whole system was immersed in liquid nitrogen (77 K) and evacuated to reach the vacuum at $10^{-5}$ bar. The crucible was heated at 40 A until Sn boiling point. In the reaction, the metallic Sn and the solvent were codeposited over half an hour. The frozen matrix, obtained on the reactor walls, was allowed to warm slowly for 1 h. After this time, the reactor was filled with extra pure nitrogen gas. After 30 min under nitrogen flow, Sn colloidal dispersions in organic media were obtained. In a typical reaction, $4.9\times10^{-5}$ mol of Sn (purchased from Aldrich) was evaporated with 100 mL of 2-propanol (dried and degassed) to obtain the Sn-Coll–2-propanol.

### Electron microscopy studies

Particle sizes for colloidal dispersions were obtained by histogram analysis of images obtained using a transmission electron microscopy (TEM) (JEOL-JEM 1200EXII) with 4 Å resolution. A drop of each colloid was placed on a dry copper grid (150 mesh) previously coated with carbon, in an inert atmosphere. TEM software Digital Micrograph™ 3.7.0 by Gatan (Pleasanton, CA, USA) was used for TEM image processing. The measurement of particle size population diameter was randomly chosen and the obtained data were represented by a histogram. Therefore, the mean particle size was fitted with normal and Gaussian curves.

### Thermogravimetric analysis

TGA experiments were carried out using a Thermogravimeter Analyzer Perkin Elmer TGA 7. All experiments were performed in a nitrogen atmosphere. All specimens were weighted in the range of 3–5 mg and were heated to 550 °C at a rate of 10 °C/min.

### UV spectroscopy

The UV absorption spectra of colloid particles (0.25%v/v) were analyzed with a spectrophotometer UV Shimadzu, Kyoto, Japan. Absorption spectra were recorded from 190 to 400 nm, using quartz cells.

### Fourier transform infrared spectroscopy

Fourier transform infrared (FT-IR) was performed in a Nicolet Nexus spectrometer at room temperature (Nicolet Instrument, Madison, WI, USA). The colloids were dried under vacuum and the samples were prepared in a KBr pellet (×2%, w/w). The spectra were carried out between 400 and 4,000 $cm^{-1}$, with an accumulation of 64 scans, collected and processed with the Omnic 5.2a software package.

### Light scattering studies

Light scattering measurements were carried out with a 90 Plus Particles Brookhaven equipment, at 25 °C, with dry and degasified 2-propanol as solvent, at 659 nm. Ten measures of 1 min each and 90 dust filter settings were performed. Measurements of colloids were taken at 1, 24, 48, 72, and 96 h. This analysis permitted the study of the Sn colloidal particle aggregation.

### Electrophoresis

Electrophoresis experiments at 1, 24, 48, 72, and 96 h were carried out with a Zeta Meter System 3.0 + (Zeta Meter, Staunton, VA, USA) at 25 °C. Quartz cells were used, rinsed previously with deionized water and after with the corresponding solvent.

## Results and discussion

Dark colloidal dispersions with different solvents used in the synthesis (2-propanol, acetone and THF) were obtained by CLD. Scheme 1 shows Sn-Colls formation, nanostructured solids, and Sn films. Frozen matrix after evaporation can be observed in Fig. 1.

Colloid stability was defined as the time in which the metallic particles remained in suspension until flocculation at room temperature [14]. Sn-Colls stability followed the tendency: 2-propanol > acetone > THF. Table 1 summarizes stability data and particle size.

A statistical study of TEM images was carried out for each colloidal system. This study consisted of the size (diameter) measurement of about 100 particles for the TEM images of the Sn-Colls, using the TEM software Digital Micrograph™ 3.7.0 (by Gatan) software. The counts were then plotted as frequency histograms using the Microcal™ Origen 6.0 software of (Microcal Software, Northampton, MA, USA). The mean particle sizes and standard deviation were also calculated.

The smaller particle size (2.5 nm) was obtained with acetone (Fig. 2) for colloids with a concentration of $4.19\times10^{-4}$mol/L. At the same concentration, colloids obtained with THF showed a higher particle size (4.7 nm) and colloids with 2-propanol showed a medium particle size of 3.0 nm. The Sn-Nps size was not significantly different from colloid concentration but there was a variation with the type of solvent used in the synthesis and showed the tendency: acetone < 2-propanol < THF.

Colloid stability depends significantly on the interaction metal–solvent, solvent nature, and particle size in suspension. This avoids the flocculation tendency of colloidal suspensions and metal particle agglomerations, thus enabling separation between particles by Van de Waals attraction forces and electrostatic repulsion curve [21].

At $2.20\times10^{-3}$ and $4.20\times10^{-4}$ mol/L, colloid stability for Sn-2-propanol was 240 and 336 h, respectively. Colloids prepared with acetone flocculated at 36 h and those prepared with THF flocculated at 24 h, due to the increase of particle agglomeration. Most of the colloids obtained by CLD are kinetically unstable, owing to the high reactivity of nanoparticles caused by the high fraction of the located atoms on the surface. Atoms on the surface have low coordination states; for this reason, they are more reactive than atoms located on the bulk. Besides, Sn-Nps are more reactive than noble metal nanoparticles. Therefore, Sn-Nps react among themselves, growing and producing strong gravitational effects with further flocculation [21].

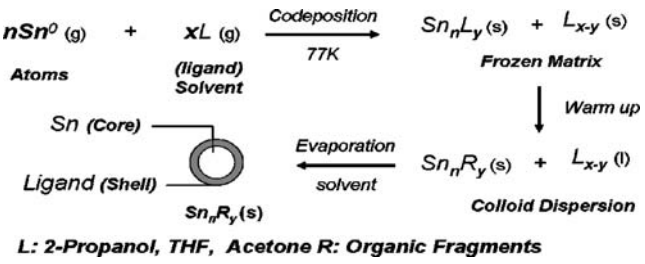


**Scheme 1** Formation of Sn colloids and nanoparticles

High-resolution transmission electron microscopy (HRTEM) measurements provided further information on the structure and the dominant morphology of the Sn particles. Figure 3b depicts a particle (corresponding to Sn-Nps-THF) in a favorable projection, which is decisive as it concerns its shape. A characteristic hexagonal periphery is observed in this image. From the atomic lattice structure, the crystallographic orientation is uniquely determined as [011]. Considering the latter, the possible low index projections of the few plausible geometries, only the cubooctahedron possesses a hexagonal outer shape in this crystallographic orientation. The shape can be identified as cuboctahedral [22–24]. Spots of filtered images determined an interplanar distance of 0.3245 nm, belonging to (200) plane and corresponding to $\alpha$-Sn (Fig. 3c).

Comparing the results obtained with Scheme 2, it can be concluded that the Sn-Nps in Fig. 3b are found in the axis zone [011] and corresponded to a cuboctahedral structure. A hard-sphere model of the cuboctahedron with regular triangular (111) facets, was observed down the [011] axis (Scheme 2b). The sets of low-index planes parallel to this axis are seen from their traces in the projections $d_{111}$ and $d_{200}$ and refer to the interplanar distances of [111] and [200], respectively.

For Sn-Nps–acetone and Sn-Nps–2-propanol, similar structures were observed. Similar features were seen for molecular clusters in which the metal cores are members of a series of "magic-number" clusters obtained by surrounding an atom with successive shells of atoms of its kind [25, 26]. In the case of metal clusters of close packed cubic (fcc), a simple model to take into account is a super-cell of bulk lattice. From the total free energy considerations, it appears that preferred shapes for such particles are closed-shell cuboctahedral, obtained through (111) faceting of a basic fcc cube [27, 28]. This type of structure was observed for Au, Ag, Ni, and Pd nanoparticles [29]. This was also found in Ge-Coll–2-propanol produced by CLD [30] and in In-Sn bimetallic particles, forming distorted cuboctahedra [31].

Electron diffraction studies for all systems showed patterns with a set of concentric rings or diffraction points or both. The measurements of the diameter of the rings allowed the evaluation of their crystalline phases. Phases were assigned by comparison of $d_{hkl}$ experimental with JCPDS reference data [32]. Table 2 summarizes the values for some representative samples and crystalline phases that

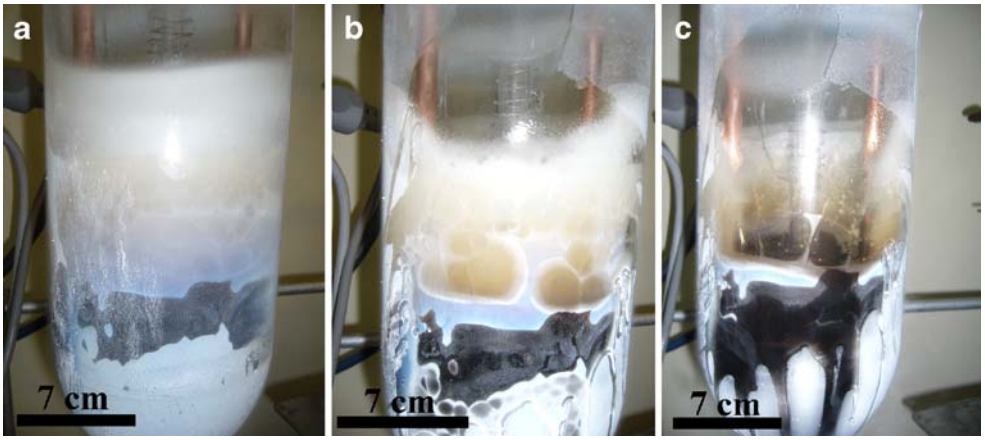


**Fig. 1** Frozen matrix of Sn-Coll–2-propanol: **a** After nucleation, **b** 1 min, **c** 1.8 min. The colors of frozen matrix are *brown* and *blue*; these colors are produced by effects of quantum size. The colloid dispersion is *black*

justify the interplanar distances, obtained from diffraction patterns showed in Fig. 4.

Analysis revealed the presence of metallic tin particles in all solvents with different crystalline phases: the determined structure corresponded to α-Sn, also confirmed by HRTEM micrographs. Particles were amorphous, with little crystallites randomly oriented, showing few diffraction rings.

Phases corresponding to SnO and $SnO_2$ oxides were not observed. Solvatation is important to avoid the oxidation of nanoparticles, and in some cases, the aggregation produces the flocculation and growth of nanoparticles.

Spectroscopic studies of Sn-Colls showed that all colloids continuously absorbed in the UV range, forming a broad peak close to 202 and 209 nm for Sn-Coll–2-propanol ($2.193\times10^{-3}$ mol/L) and Sn-Coll–THF ($2.193\times10^{-3}$ mol/L), respectively (Fig. 5). These colloids present properties deriving from particle size in suspension, such as incident light dispersion by successive reflexions and refractions, known as the Tyndall effect, and optical properties corresponding to their metallic nature. However, many aspects can differ with respect to metals, understood as compact materials. Metallic nanoparticles can be considered an intermediate state between atoms and compact material [33]. These results are in agreement with the theoretic spectra calculated by Creighton et al. applying the Mie Theory. The Creighton calculations were performed considering spherical particles of 10 nm. The spectrum was calculated at vacuum, and in dielectric medium with water refractive index. Creighton predicts continuous absorption in the UV region, which increases until the formation of a broad band with a maximum close to 200 nm [34], similar to our colloids. Although this absorption cannot be assigned to plasma absorption, it is characteristic of the metallic state and corresponds to superimposed interband transitions. The previous behavior indicated an associated effect of quantum size, typical of particles with nanometer dimensions in which the electrons are confined to small crystalline structures of a few hundred atoms and are not free as in the bulk state.

**Table 1** Sn-Nps stability and particle size

| Solvent | Concentration mol/L | Size (nm) | Frozen matrix Color | Colloid color | Stability (h) |
|---|---|---|---|---|---|
| Acetone | $4.192\times10^{-4}$ | 2.510 | Brown | Black | 36 |
| | $2.043\times10^{-3}$ | 2.753 | Brown | Black | 1 |
| THF | $4.297\times10^{-4}$ | 4.749 | Brown | Black | 24 |
| | $2.261\times10^{-3}$ | 4.870 | Brown | Black | 1 |
| 2-propanol | $4.209\times10^{-4}$ | 3.007 | Brown, blue | Black | 336 |
| | $2.193\times10^{-3}$ | 3.108 | Brown, blue | Black | 240 |

UV measurement exhibited absorption bands for Sn-Coll–THF at 209 nm and for Sn-Coll–2-propanol, this band occurring at lower wavelength (202 nm). This blue-shift is due to quantum effects produced by the smaller particle size in suspension.

On the other hand, the Sn-Coll–acetone spectrum showed a strong and broad absorption band located at 190–350 nm. In this case, many acetone molecules interact with the nanoparticle surface forming a shell. If the solvent molecule has a double bond or carbonyl group such as acetone, the solvent–nanoparticle system acts as a true chromophore, exhibiting n-$\Pi^*$ transitions, responsible for strong absorption, as seen for Sn-Coll–acetone (Fig. 5).

In order to achieve a better understanding of the coagulation process, a study of light scattering along time was carried out. An absorption peak close to 198 nm was used as coagulation criterion. The spectra were recorded at different times (Fig 6) and absorption at 198 nm was plotted vs time, as shown in Fig. 7. An exponential decay of maximum absorbance was observed according to equation 1. The pre-exponential factor of this equation indicated that a fraction flocculates and the other remains in solution.

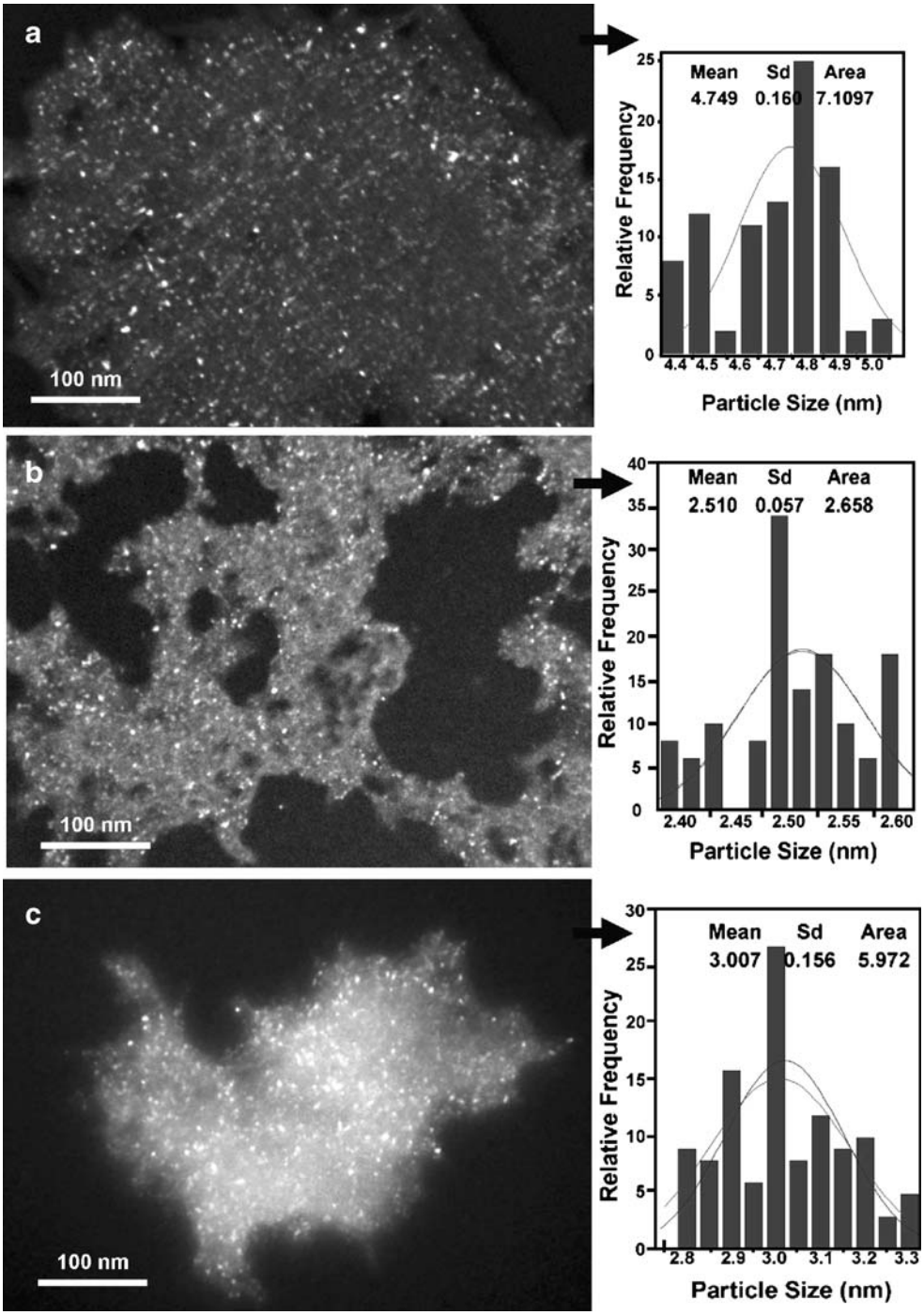


**Fig. 2** TEM micrograph of dark field and histogram: **a** Sn-Coll–acetone, **b** Sn-Coll–THF, **c** Sn-Coll–2-propanol

Absorbance decreases exponentially due to flocculation of the biggest particles or by fractal aggregate formation. This coincided with the experimental observations. Interparticle collisions are due to substantial agglomeration, especially in colloids where repulsive interactions are not present or are weak. Apparently, colloids prepared in this way possess a critical concentration below which they become relatively stable because the collisions are less effective.

At 286 and 240 nm, Sn-Coll–2-propanol showed two bands and Sn-Coll–THF showed one band at 283.15 nm (Fig. 5). These bands appeared when the particles in suspension were aggregated. As a result, the extinction band decreases corresponding to particle plasmons without aggregation. A new band appeared at higher values of λ, due to plasmons of aggregated particles. The position of this second band is related to aggregation mechanism [35, 36].

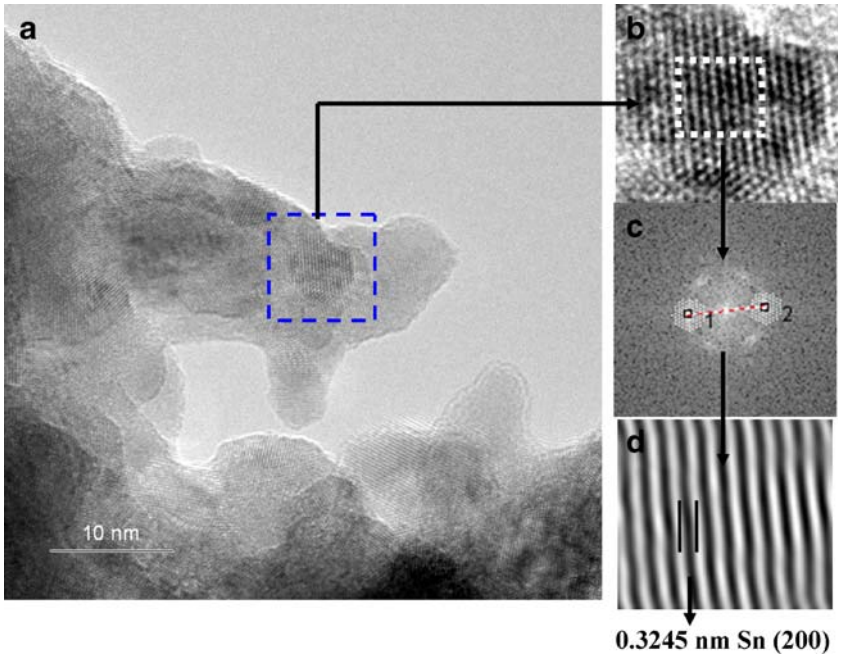


**Fig. 3** HRTEM micrograph showing: **a** Sn-Nps–THF, **b** image showing cuboctahedral Sn-Nps, **c** digital mask filtering on the corresponding FFT provided us the clean image of the particle, **d** clusters plane Sn (200)

To explain the aggregation phenomena observed in UV spectra, light scattering measures for Sn-Coll–2-propanol colloids were carried out. Corresponding data are plotted in Fig. 8.

Measurements were performed at different times from 2 to 96 h, obtaining an effective diameter of 350 nm at 2 h. The aggregate diameter increased to 448 nm at 24 h, and at 48–96 h, the aggregate diameter increased to 630–675 nm. Globular aggregates of fractal type for Sn-Coll–2-propanol were detected along time. These aggregates continue, growing to critical size by effects of zeta potential reduction, producing colloid flocculation. On the other hand, the aggregation mechanism of metallic particles depends closely on the charge density over the particle surface. At high concentrations of absorbate, charge density is greatly reduced, producing a controlled colloidal aggregation by diffusion (diffusion-limited colloid aggregation).

The maximum value obtained in effective diameter measurement corresponds to the maximum growth of fractal aggregates formed in colloidal dispersion. Solvent effects and interactions between fractals produce aggregation, so that fractal formation with major dynamic volume explains the obtained values between 48 and 96 h. The aggregation mechanism of metallic particles depends mainly on their charge density. The decreasing zeta potential along time (Fig. 9) revealed that the decrease permits contact between particles, due to vanishing repulsion effects, producing particle agglomeration. This phe-

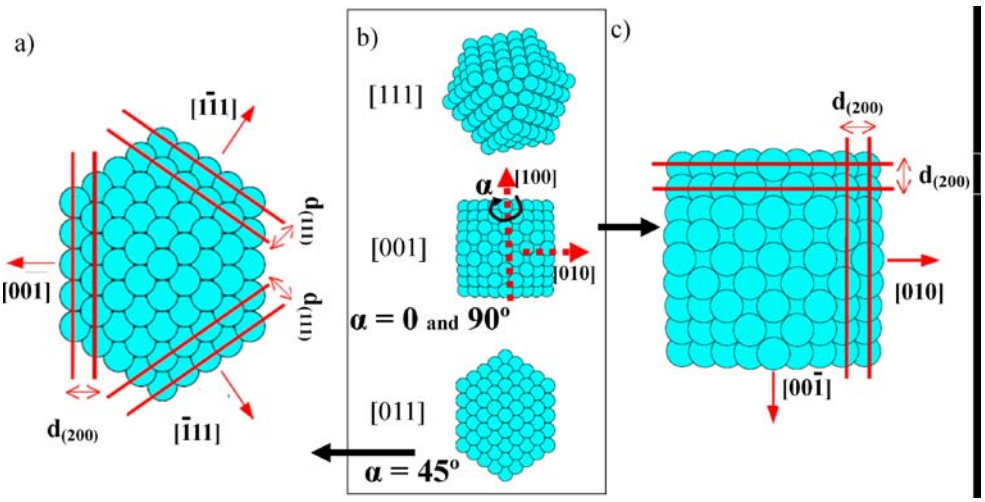


**Scheme 2** **a** Hard-sphere model of the cuboctahedron with regular triangular (111) facets, observed down the [011] axis, **b** scheme of a 309-atom cuboctahedral cluster seen in three different zone axis directions: [111], [001] and [011]. The cluster was tilted around the x axis ([100]) from [001] to [010] zone axis, for [001] and [010] zone axis ($a$=0 and 90°, respectively), for [011] zone axis ($a$=45°). **c** Same cuboctahedron as in **a**, but observed down [001]

**Table 2** Crystalline phases and assignments for Sn-Coll

| Colloids | D(hkl) exp (Å) | Phase | d(hkl) ref (Å) |
|---|---|---|---|
| Sn-2-propanol | 3.742 | Sn-(α) (111) | 3.751 |
| | 2.284 | Sn-(α) (220) | 2.294 |
| Sn-THF | 3.758 | Sn-(α) (111) | 3.751 |
| | 2.321 | Sn-(α) (220) | 2.294 |
| | 1.472 | Sn-(α) (133) | 1.489 |
| Sn-Acetone | 3.761 | Sn-(α) (111) | 3.751 |
| | 2.299 | Sn-(α) (220) | 2.294 |

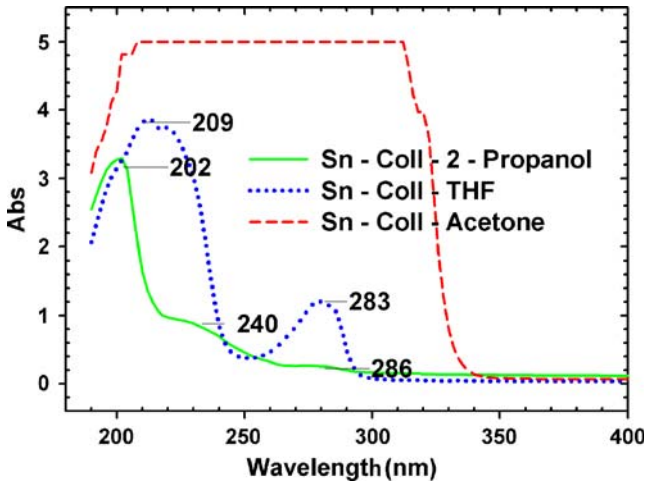


**Fig. 5** UV Spectra of Sn-Colls obtained with: 2-propanol, THF, and acetone

nomenon explains the fractal aggregate formation along time.

There are two fundamental mechanisms for colloidal particle stabilization: one of a steric type in which organic fragments attached to the particle surface play a fundamental role and the other, of an electrostatic repulsion type due to absorbed ions. In the case of our experiment, particle formation occurs by metal atoms clustering in organic media where the steric factor seems to be the most important. However, a previous report of electrophoresis studies also suggests a weak electrostatic contribution to the stabilization [37].

Figure 10 shows the FT-IR spectra of nanostructured solids. Representative vibrations are summarized in Table 3.

The Sn-Nps-THF, presented $\upsilon_{(O-H)}$ characteristic bands at 3,421 $cm^{-1}$ and absence of $\upsilon_{(C-H)}$ 2,971 $cm^{-1}$, attributable to solvent presence. In addition, attributable bands to olefins, at $\upsilon_{(C-H)}$ 1,467 $cm^{-1}$ can be observed. $\upsilon_{(C-O)}$ absorption at 1,089 $cm^{-1}$ was shifted to 1,022 $cm^{-1}$ for Sn-Nps-THF. Far FT-IR spectrum showed $\upsilon_{(Sn-O)}$ absorption at 454 $cm^{-1}$. According to Allan et al. [38], metal alkoxides, $M(OR)_n$ (R:alkyl), exhibit $\upsilon_{(C-O)}$ absorptions close to 1,050 $cm^{-1}$ and $\upsilon_{(M-O)}$ at 600–400 $cm^{-1}$. Infrared spectra have been reported for several alkoxides of Er(III) [39] and isopropoxides of rare-earth metals [40]. According to absorption bands, two possible structures were suggested: (1) ring-opening, with generation of O-H bond, where the interactions are produced by Sn-O, and (2) THF-O interaction on metal surface, without ring-opening. Possible adducts of Sn-Nps-THF are shown in Fig. 10a. These results were different to those published by Segura et al. [43] for the synthesis of germanium nanoparticles, who obtained adducts with metal-carbon double bond (M = C) between the metal and the solvent (THF) by CLD [41].

For Sn-Nps-2-Propanol (spectrum of solid sample), $\upsilon_{(Sn-O)}$ characteristic band at 443 $cm^{-1}$ can be observed. Shifted $\upsilon_{(O-H)}$ band at 3,437 $cm^{-1}$ was broader and stronger, indicating that bond length decreased in the solid. This band confirmed the metal–oxygen interaction by absence of $\upsilon_{(Sn-C)}$ band at 532–576 $cm^{-1}$ [42, 43]. The structure proposed for Sn-Nps-2-propanol surface is shown in Fig. 10a. FT-IR spectra of acetone and Sn-Nps–acetone solids were compared, the corresponding $\upsilon_{(C=O)}$ band at 1,703 $cm^{-1}$ was shifted to 1,716 $cm^{-1}$; furthermore, $\upsilon_{(O-H)}$ characteristic absorption of solid appears at 3,429 $cm^{-1}$. For Sn-Nps–acetone, two structures were proposed: (1) acetone interacts directly with metallic surface and (2) organic

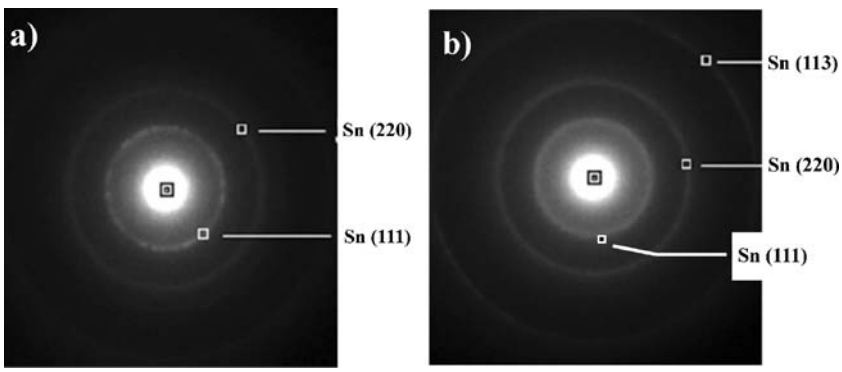


**Fig. 4** Electron diffraction pattern: **a** Sn-Coll–2-propanol, **b** Sn-Coll–THF

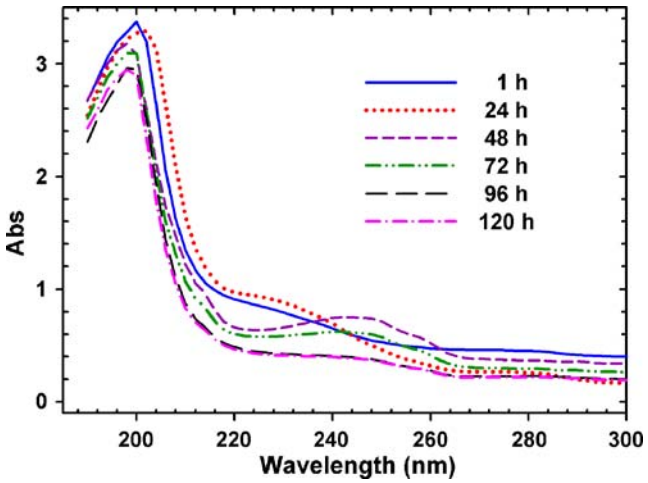


**Fig. 6** UV spectra of Sn-Coll–2-propanol ($4.209\times10^{-4}$ mol/L) along time

molecule is reduced to alcohol; both structures are shown in Fig. 10a. Proposed structures evidenced an interaction between oxygen of organic molecule with active metallic surface. The Nps-shell is composed of a solvent carbon chain. A functional group with a higher electron density interacts with Sn-core, which would explain the positive charge of particles (Fig. 10b).

Sn-Nps showed a good thermal stability. Sn-Nps–2-propanol and Sn-Nps–THF adducts have similar decomposition temperature $T_d$, at 303.37 °C and 304.98 °C, respectively, with a mass loss of 3.47% and 3.7% (Table 4). These values are different from those reported by Cardenas et al. [44]. Sn-Nps–acetone was less stable in comparison to the above mentioned, showing a decomposition temperature and mass loss of 298.92 °C and 3.56%, respectively.

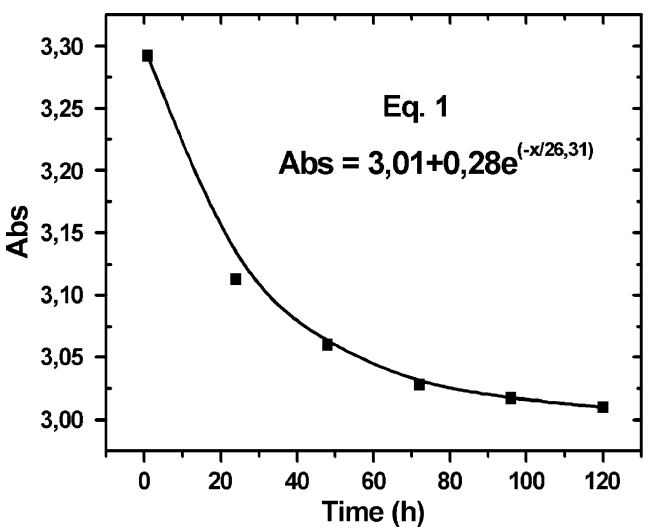


**Fig. 7** Absorbance vs time of treatment for Sn-Coll–2-propanol ($4.209\times10^{-4}$ mol/L)

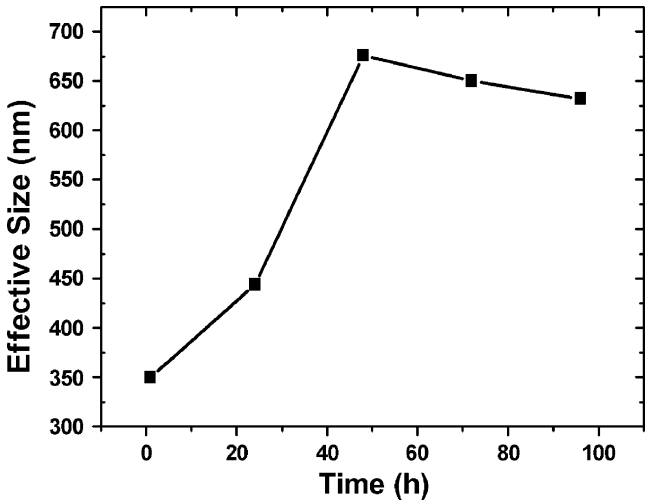


**Fig. 8** Light scattering measurements of Sn-Coll–2-propanol along time

In all cases, mass loss of studied adducts are similar and ranged between 3.4 and 3.7% and $T_d$ between 304.98 and 298.92 °C. Similarities found in $T_d$ were due to Sn-O interaction, evidenced by FT-IR analysis, for all colloids.

## Conclusions

CLD is an effective method to obtain Sn–THF, Sn–acetone and Sn–2-propanol colloidal nanoparticles, ranged between 2.5 and 4.8 nm. UV spectroscopy analysis showed that Sn-Colls are relatively unstable due to the decrease of characteristic absorption bands along time. UV results also showed that nanoparticles absorb between 200 and 300 nm

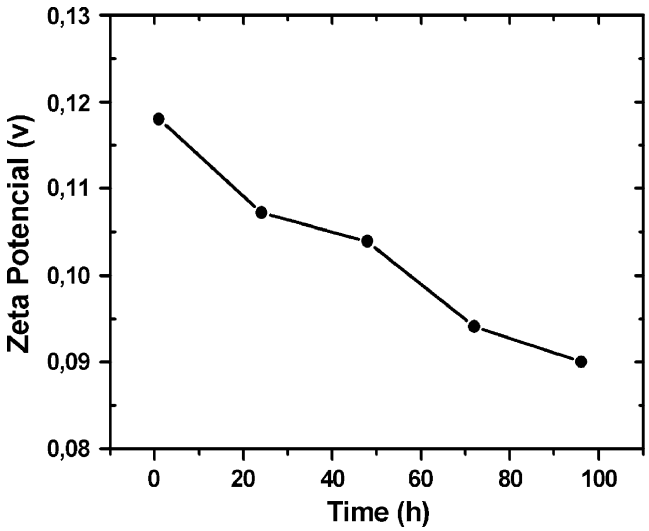


**Fig. 9** Zeta potential of Sn-Coll–2-propanol ($4.2\times10^{-4}$ mol/L) along time. Particles charge determined by electrophoretic was positive

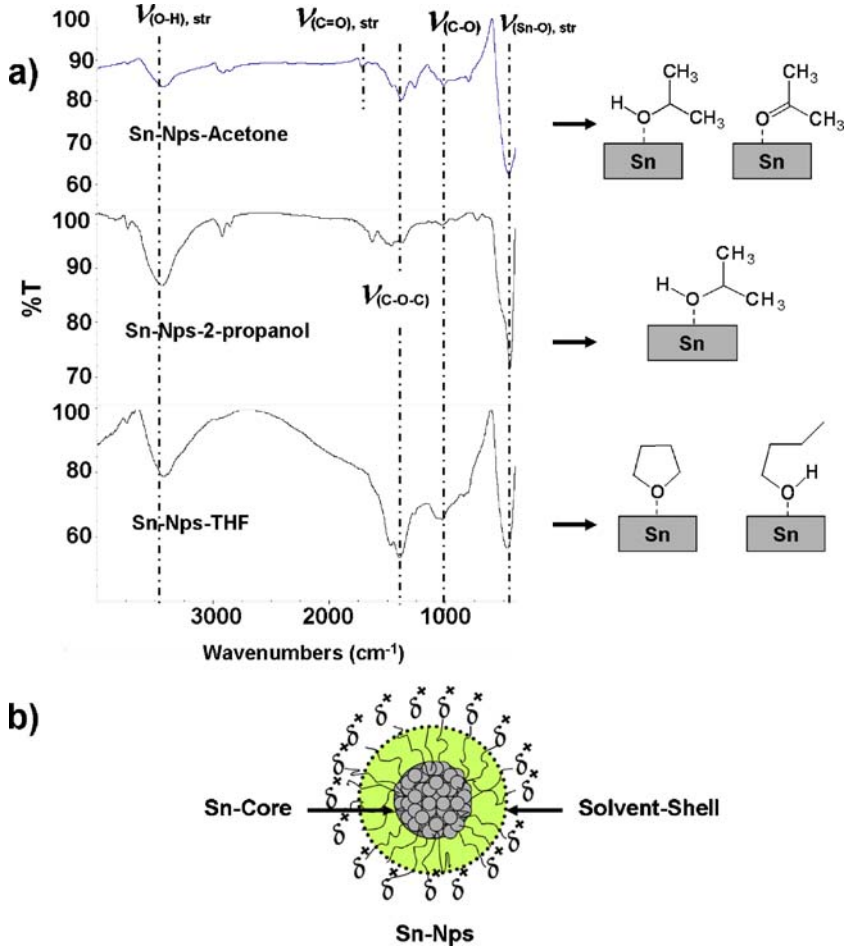


**Fig. 10** **a** FT-IR spectra for Sn-Nps–solvent. Solvent: 2-propanol, acetone, THF. Proposed structures for Sn-Nps surfaces. **b** Representation of Sn-Nps–solvent (core-shell)

**Table 3** FT-IR Bands of the active solid

| Solid | υ ($cm^{-1}$) Solid | υ ($cm^{-1}$) Solvent | FT-IR assignment |
|---|---|---|---|
| Sn-Nps–acetone | 3,429 | – | $\upsilon(O-H)_{sym.\ str}$ |
| | 1,716 | 1,703 | υ(C = O) |
| | 1,378 | – | υ(C-O-M) |
| | 1,014 | 1,124 | $\upsilon(C-O)_{sym\ tors}$ |
| | 454 | – | $\upsilon(M-O)_{sym.\ str}$ |
| Sn-Nps-2-Propanol | 3,437 | 3,345 | $\upsilon(O-H)_{sym.\ str}$ |
| | 1,369 | – | υ(C-O-M) |
| | 1,015 | 1,093 | $\upsilon(C-O)_{sym\ tors}$ |
| | 443 | – | $\upsilon(M-O)_{sym.\ str}$ |
| Sn-Nps-THF | 3,421 | – | $\upsilon(O-H)_{sym.\ str}$ |
| | $1{,}390^{++}$ | $1{,}363^{+}$ | $\upsilon(C-O-M)^{++}$ $\upsilon(C-O-C)^{+}$ |
| | 1,022 | 1,089 | $\upsilon(C-O)^{b}_{sym\ tors}$ |
| | 465 | – | $\upsilon(M-O)^{a}_{sym.\ str}$ |

*M* metal
[a] Symmetrical stretching
[b] Symmetrical torsion

in the UV region, showing the quantum confinement effect. Particle size distribution depends on the initial colloid concentration; the sizes found with the different solvents showed the following tendency: Sn-Nps–acetone < Sn-Nps-2-propanol < Sn-Nps-THF. Colloid stability showed the tendency: Sn-Colls-2-Propanol > Sn-Colls-Acetone > Sn-Colls-THF. In all cases, when the colloid concentration is increased, stabilization time also decreases. Colloids are composed by α-Sn phase according to electron diffraction patterns with all solvents used. Decreasing of zeta potential is responsible for fractal growth in colloids, producing flocculation in colloidal dispersions; these fractals were also evidenced in UV spectra by bands appearing at a higher wavelength. FT-IR analysis showed Sn-O interaction in all solvents, producing Sn-Nps with a positive shell.

**Table 4** Thermogravimetric analyses

| Solid | Td (°C) | Weight loss (%) |
|---|---|---|
| Sn-Nps-2-propanol | 303.37 | 3.47 |
| Sn-Nps-THF | 304.98 | 3.70 |
| Sn-Nps–acetone | 298.92 | 3.56 |

**Acknowledgements** We are grateful to CONICYT (AT-24071064; 21050655), AGCI, and CIPA for scholarship grants. Sincere thanks are also given to Mecesup Project UCHO (*Beca reforzamiento de la red nacional de programas de doctorado*), Graduate School of *Universidad de Concepción*, FONDECYT 1040456 and Innova Bío-Bío for the financial support. Also, thanks to *Serveis Cientificotècnics* of the *Universitat de Barcelona*, Spain, for the use of the HRTEM.

## References

1. Sun Y, Xia Y (2002) Science 298:2176
2. Tan Y, Dai X, Li Y, Zhu DJ (2003) Mater Chem 13:1069
3. Turkevich J, Kim G (1970) Science 169:873
4. Hongjin J, Kyoung-sik M, Hai D, Fay H, Wong CP (2006) Chem Phys Lett 429:492
5. Klabunde KJ, Li YX, Tan BJ (1991) Chem Mater 3:30
6. Reetz MT, Helbig W (1994) J Am Chem Soc 116:7401
7. Tano T, Esumi K, Meguro K (1989) J Colloid Interf Sci 133:530
8. Chem WX, Lee JY, liu Z (2002) Chem Commun 2588
9. Yu WY, Liu HF (1998) Chem Mater 10:1205
10. Klabunde KJ, Youngers G, Zuckerman E, Tan B (1992) J Solid State Inorg Chem 29:227
11. Klabunde KJ (1980) Chemistry of free atoms and particles. Academic, London
12. Stoeva SI, Klabunde KJ, Sorensen CM, Dragiera I (2002) J Am Chem Soc 124:2305
13. Cárdenas G, León Y, Moreno Y, Peña O (2006) Colloid Polym Sci 284:644
14. Lavayen V, O'Dwyer C, Santa Ana MA, Mirabal N, Benavente E, Cárdenas G, González G, Sotomayor Torres CM (2007) Appl Surf Sci 253:3444
15. Cárdenas G (2005) J Chil Chem Soc 50:603
16. Sánchez S (2004) Opt Pur y Apl Vol 37 Núm 2
17. Korotcenkov G (2005) Sensors and Actuators B 107:209
18. Fan H, Reid S (2003) Chem Mater 15:564
19. Kim HW, Shim SH, Lee C (2006) Ceram Int 32:943
20. Lima CA, Oliva R, Cárdenas G, Silva EN, Miranda LC (2001) Mater Lett 51:357
21. Cárdenas G, Segura R, Reyes-Gasga J (2004) Colloid Polym Sci 282:1206
22. Arbiol J, Cabot C, Morante JR, Chen F, Liu M (2002) ApplPhys l Lett 18:3449
23. Arbiol J, Peiró F, Cornet A, Morante JR, Pérez-Omil JA, Calvino, Mat JJ (2002) Sci Eng B 91–92:534
24. Arbiol J, Cirera A, Peiró F, Cornet A, Morante JR, Delgado, Calvino JJ (2002) Appl Phys Lett 80:329–331
25. Schmid G (Ed) (1994) Clusters and colloids: from theory to applications. *VCH*, Venheim
26. Volokitin Y, Sinzig J, de Jongh LJ, Schmid G, Vargaftik MN, Moiseev I (1996) Nature 384:621
27. Malm J-O, O'keefe MA (1997) Ultramicroscopy 68:13
28. Casanove M-J, Lecante P, Snoeck E, Mosset A, Roucau C (1997) Journal of Physics III France 7:505
29. Buffat P-A, Flüeli M, Sopycher R, Stadelmenn P, Borel J-P (1991) Faraday Discuss 92:173
30. Segura R, Cárdenas G (2008) J Cryst Growth 310:495
31. Bhattacharya V, Chattopadhyay K (2004) Mat Sci Eng A 375:932
32. Powder Diffraction File, Inorganic Phases, JCPDS (1997), International Centre for Diffraction data, Pennsylvania, USA
33. Henglein A, Bunsenges B (1995) Phys Chem 99:903
34. Creighton J, Eadon D (1991) J Chem Soc Faraday Trans 87:3881
35. Kubo R (1962) J Phys Soc Jpn 17:975
36. Marker M (1985) J Coll Interface Sci 105:297
37. Cárdenas G, Klabunde KJ, Dale E (1986) Langmuir 3:986
38. Allan KA, Gowenlock BG, Lindsell WE (1973) J Organometal Chem 55:229
39. Almenningen A, Haaland A, Motzfeldt T (1967) J Organometal Chem 7:97
40. Harrison PG, Healy MA (1973) J Organometal Chem 51:153
41. Pettinari C, Lorenzotti A, Sclavi G, Cingolani A, Rivarola E, Colapietro M, Cassetta A (1995) J Organometal Chem 496:69
42. Amalric-Popescu D, Bozon-Verduraz F (2001) Catal Today 70:139
43. Segura R, Reyes-Gasga J, Cárdenas G (2005) Colloid Polym Sci 283:854
44. Cárdenas G, Alvial M, Klabunde KJ, Pantoja O, Zoto H (1994) Colloid Polymer Science 272:310